Synergetic Peroxidase-Mimic Catalytic Activity of Noble-Metal-Decorated Lithium Niobate Nanozymes for Potential Biological Applications

Ana-María Pablo-Sainz-Ezquerra, Rachael Taitt, Florian Riporto, Yannick Mugnier, Pyria Mariathomas, Ronan Le Dantec, Mimoun Aouine, Christophe Geantet, Rajesh Ramanathan, Vipul Bansal, et al.

Synergetic Peroxidase-Mimic Catalytic Activity of Noble Metal-Decorated Lithium Niobate Nanozymes for Potential Biological Applications

*Ana-María Pablo-Sainz-Ezquerra[1,3], Rachael Taitt[1], Florian Riporto[2], Yannick Mugnier[2], Pyria D. Mariathomas[3], Ronan Le Dantec[2], Mimoun Aouine[4], Christophe Geantet[4], Rajesh Ramanathan[3], Vipul Bansal[3], Yann Chevolot[5], Virginie Monnier[1]**

[1]Univ Lyon, Ecole Centrale de Lyon, CNRS, INSA Lyon, Université Claude Bernard Lyon 1, CPE Lyon, INL, UMR5270, 69130 Ecully, France.

[2]Université Savoie Mont Blanc, SYMME, F-74000 Annecy, France.

[3]Sir Ian Potter NanoBioSensing Facility, NanoBiotechnology Research Laboratory, RMIT University, Melbourne, Victoria, 3000, Australia.

[4]Univ Lyon, Université Claude Bernard Lyon 1, CNRS, IRCELYON, Villeurbanne, F-69626, France.

[5] Univ Lyon, CNRS, INSA Lyon, Ecole Centrale de Lyon, Université Claude Bernard Lyon 1, CPE Lyon, INL, UMR5270, 69130 Ecully, France

*E-mail: virginie.monnier@ec-lyon.fr

Keywords: Hybrid nanoparticles, lithium niobate, noble metal, peroxidase, synergetic effect

Abstract

In this paper, we report a simple, facile, and efficient method to obtain $LiNbO_3$/Au and $LiNbO_3$/Pt nanoparticles composed of $LiNbO_3$ NPs (LN NPs) (30 nm) and ultrasmall nanoparticles (< 5 nm, seeds) of Au and Pt, respectively. The synthesis of the nanocomposites followed a simple layer-by-layer method introducing branched polyethyleneimine (BPEI) as a linker. By varying the volume of metal seeds dispersion added to the LN coated with BPEI, the loading of metal on the surface of the LN is controlled. The morphology of the as-prepared composite is characterized by TEM, EDS and DLS. Its applicability as peroxidase-mimics is investigated and compared to the separated counterparts (LN NPs, LN@BPEI, AuSeeds, PtSeeds and a simple mixture of LN NPs and metal seeds). The synthesized nanoparticles follow the Michaelis-Menten kinetic model with enhanced catalytic activity compared to the metal seeds alone. This intrinsic peroxidase activity

made them promising candidates for applications in biomedicine. In particular, the low Michaelis constant K_m and high maximum velocity V_{max} for the H_2O_2 are of great interest for H_2O_2 sensing and generation of reactive oxygen species for antimicrobial applications.

1 Introduction

The ability of certain inorganic nanoparticles to catalyze reactions that are typically driven by natural enzymes has seen the emergence of a new field called nanozymes.[1] To date, a range of nanoparticles with different compositions including metals, metal oxides, metal sulfides etc. have been reported for their potential to catalyze reactions that mimic the activity of peroxidase, oxidase, catalase, superoxide dismutase, glycosidase, protease, phosphatase, phosphodiesterase, and laccase.[2] Further, tunability of the nanozyme activity has also been achieved by modifying the properties of the nanoparticles (size, shape, composition), reaction conditions (pH, temperature, concentration of nanoparticles and/or substrates), and use of external stimuli (light or magnetism). Although the field of nanozymes is relatively new, most reports, until recently, focused on employing monometallic nanoparticles as nanozymes.[3,4] Recent studies have outlined the importance of combining two nanoparticles to create bimetallic nanozymes that show unique properties due to the synergetic effect that is otherwise not observed in the monometallic nanozymes.[5] For instance, hybrids of Cu-Pt and Cu-Pd showed the ability to drive the oxidation of 3,3',5,5'-tetramethylbenzidine (TMB), a common peroxidase enzyme substrate, to form a yellow colored diimine derivative product.[6] This was interesting as nanozymes are typically only

capable of oxidizing TMB to form a blue charge transfer complex product. Other examples have also reported increased H_2O_2 reduction current when employing Au-Fe_3O_4 heterodimers compared to Au or Fe_3O_4.[7] Similarly, PtPd-Fe_3O_4 hybrids show superior catalytic activity when compared to horseradish peroxidase (HRP).[5] Based on these studies, it is clear that to obtain interesting properties and achieve superior catalytic activities, it is critical to choose the right combination of materials.

To this end, $LiNbO_3$ (LN) is an interesting material as it has a non-centrosymmetric structure that confers outstanding nonlinear optics, pyroelectric and piezoelectric properties, making it ideal for numerous applications in optics, batteries and optical communications.[8–10] At the nanoscale, LN NPs present low toxicity and lack phase-matching conditions, making them an excellent candidates for bio-imaging and photo-triggered drug delivery.[11,12] Other features include its semiconducting and ferroelectric properties that enhance catalysis and photocatalysis, especially in redox reactions. These properties favour charge separation and polarization-induced facile adsorption.[13] For instance, illuminating LN with UV light ($\lambda < 333$ nm) produces electrons and holes favouring the production of hydroxyl and superoxide anion radicals, leading to the oxidation of organic compounds.[14] Although the presence of oxygen vacancies is anecdotic, preferential

oxygen fixation occurs in positively polarized regions on the LN surface.[15,16] To date, LN has been combined with natural enzymes such as glucose oxidase to develop sensors.[17] To our best knowledge, there are no studies that have combined LN with nanozymes to create a hybrid system.

In the current work, we focus our effort to create LN NPs coated with AuSeeds (< 5 nm) and PtSeeds (< 5 nm) with fine control over the surface coverage of the metal seeds by exploiting electrostatic forces. The addition of noble metal seeds on LN using a simple layer-by-layer approach to create LN/Au and LN/Pt hybrid nanoparticles would allow for improving the weak electronic mobility in LN thereby making redox reactions favourable, which is otherwise not favoured.[17] The hybrids showed the ability to oxidize common peroxidase substrates in the presence of H_2O_2 as a co-substrate suggesting that both nanozymes show peroxidase-mimic catalytic activity. In depth analysis of the peroxidase mimics showed that the interface formed as a result of the chemical link created by BPEI between the LN NPs and the AuSeeds or PtSeeds is critical to enhance the catalytic activity. The scope of this study is to investigate the synergetic enhancement in the peroxidase-mimic activity due to the metal/metal oxide interface. Although this paper is not focused on a specific application, we believe that these hybrid nanoparticles may be suitable for a variety of biological functions, including biosensing, antimicrobial and cancer

therapy, protection against cell damage or reduction of inflammation for which peroxidase-mimic nanozymes have been found useful.[3] Some potential applications are thus detailed at the end of the paper.

2 Experimental Section

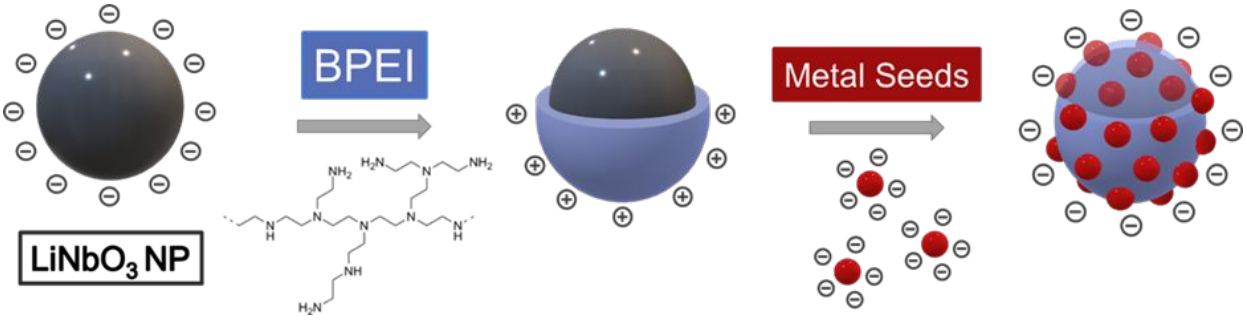

Scheme 1. Layer-by-layer synthesis method for LN/Au and LN/Pt hybrid NPs.

A detailed list of materials and methods is given in the Supplementary Material (SI). $LiNbO_3$ NPs (LN NPs) were synthesized by non-aqueous solvothermal alkoxide process, as previously described.[18] The obtained LN NPs were dried and redispersed in water. Subsequently, the hybrid nanoparticles of LN NPs and metal seeds were assembled through electrostatic interactions, as we previously described (**Scheme 1**).[19] In brief, branched polyethylenimine (BPEI) was attached to the LN NPs, obtaining LN@BPEI NPs with positive surface charge. We synthesized separately negatively charged metal seeds of Au and Pt (ultrasmall nanoparticles, < 5 nm) through a salt-reduction method using tetrakis-(hydroxymethyl)-phosphonium chloride (THPC) as the surfactant

and reductor in the dark.[20] The negatively charged metal seeds and the positively charged LN@BPEI NPs were mixed for 30 min and aged for 72 h. In addition, different loadings of metal seeds onto LN@BPEI NPs were obtained by varying the volume ratio between metal seeds dispersion to LN@BPEI dispersion. The hybrid nanoparticles were washed several times through centrifugation to remove any unbounded metal seeds and unreacted species and then studied using a suite of colloidal and material characterisation methods.

The peroxidase mimics of the hybrid nanoparticles of LN/Au and LN/Pt were assessed by exposing a fixed amount of LN/Au and LN/Pt to TMB substrate in the presence of H_2O_2. The change in absorbance was measured over time. We optimized the pH and temperature and obtained the Michaelis-Menten steady-kinetic parameters while independently varying TMB and H_2O_2 substrates.

3 Results and Discussion

3.1 Characterization of the NP constructs (LN, LN@BPEI, AuSeeds and PtSeeds)

The diameter of LN NPs synthesized by a non-aqueous solvothermal method was determined by TEM (**Figure 1A-1A1**, **Table 1**) and DLS. The average TEM diameter calculated from 200 LN NPs was 30.4 ± 8.6 nm and the corresponding hydrodynamic diameter from DLS measurements

was 114.2 ± 1.7 nm (**Table 1**). The broad distribution of the TEM diameter could be attributed to the platelet-like morphology of LN NPs which makes its estimation difficult due to the possible inclinations on the TEM grid and a given size distribution along each crystallographic direction.[18] The zeta potential was around −40 mV in water leading to a stable LN NPs dispersion. This negative zeta potential can be attributed to the uncoordinated –OH groups on the LN surface, which are commonly observed on the surface of oxide nanoparticles.[19] With X-Ray Diffraction, it was previously evidenced that the LN NPs were monocrystalline with the expected trigonal R3c structure of bulk $LiNbO_3$.[18,19] The Li/Nb atomic ratio was determined by ICP-AES, leading to a ratio of 1.02, which is close to the theoretical expected value in $LiNbO_3$.[21] Following BPEI adsorption on LN NPs, the LN@BPEI NPs showed blurred edges, which may be attributed to the presence of BPEI polymer on their surface (**Figure 1B-1B1**). The hydrodynamic diameter of LN@BPEI NPs was 147.6 ± 2.8 nm (**Table 1**), an increase of ~29% compared to the native LN NPs which suggests the successful adsorption of BPEI. This was supported by the zeta potential of +39.4 ± 3.6 mV where the presence of protonated $–NH_2$ groups from the BPEI reversed the charge from negative to positive.[22]

AuSeeds and PtSeeds were synthesized by the salt reduction method using THPC as a reducer (**Figure 1C-1C1 and Figure 1D-1D1**). The average diameter of the AuSeeds calculated from 200 NPs observed by TEM was 2.0 ± 0.8 nm (**Table 1**). The diameter in the case of PtSeeds was slightly higher, with an average value of 3.1 ± 0.6 nm. UV-Vis absorption spectroscopy did not reveal any plasmon band further confirming that the average diameter of the metal seeds was below 5 nm.[20] The hydrodynamic diameter for AuSeeds and PtSeeds were 36.0 ± 8.5 nm and 135.7 ± 6.6 nm, respectively (**Table 1**). The THPC coating and the solvating layer of nanoparticles associated with the presence of some aggregates may explain the difference in TEM-determined diameter and DLS hydrodynamic diameter in the case of AuSeeds. For PtSeeds, the presence of aggregates (as seen in the TEM image, **Figure 1D-1D1**) may be responsible for a considerable increase in the hydrodynamic diameter measured by DLS.[23] Both metal seeds showed a negative zeta potential in water due to the presence of THPC on their surface.[20]

Table 1. TEM diameter, hydrodynamic diameter, and zeta potential values of LN NPs, LN@BPEI NPs, AuSeeds and PtSeeds.

Sample name	TEM diameter (nm) ± SD	Hydrodynamic diameter (nm) ± SD	Zeta potential (mV) ± SD
LN	30.4 ± 8.6	114 ± 2	-43 ± 1
LN@BPEI	29.6 ± 8.4	148 ± 3	+39 ± 4
AuSeeds	2.0 ± 0.8	36 ± 9	-12 ± 6
PtSeeds	3.1 ± 0.6	136 ± 7	-15 ± 2

3.2 Characterization of LN/Au and LN/Pt hybrid NPs

Au and Pt-coated LN NPs were prepared by an electrostatic assembly of the individual constructs while employing oppositely surface charged LN@BPEI particles and noble metal seeds. TEM images of LN/Au and LN/Pt NPs prepared with different noble metal seeds to LN ratios are shown in **Figure S1** (**Supporting information**) and the corresponding hydrodynamic diameters and zeta potential values are presented in **Table 2**.

Table 2. TEM diameter of metal seeds onto LN@BPEI, hydrodynamic diameter and zeta potential values of LN/Au and LN/Pt NPs measured in water.

Sample name	TEM diameter of metal seeds onto the LN@BPEI (nm) ± SD	Hydrodynamic diameter of hybrid NPs (nm) ± SD	Zeta potential of hybrid NPs (mV) ± SD
LN/Au1	2.4 ± 0.8	234 ± 9	+25 ± 1
LN/Au2	2.5 ± 0.7	164 ± 1	-29 ± 0
LN/Au3	3.1 ± 0.8	161 ± 2	-32 ± 0
LN/Pt1	2.5 ± 0.6	176 ± 3	+23 ± 2
LN/Pt2	2.5 ± 0.5	367 ± 2	-13 ± 1

The deposition of AuSeeds on LN@BPEI NPs does not significantly increase the diameter in TEM when compared to the initial AuSeeds (see **Table 1**). However, a brownish supernatant, corresponding to free AuSeeds was observed for LN/Au3 after the first centrifugation step, indicating the saturation of LN@BPEI surface with the AuSeeds. Moreover, a slight increase in the TEM diameter is observed for AuSeeds in LN/Au3. This diameter increase may come from

the reduction and coalescence of the AuSeeds on the surface of LN@BPEI as the NH_3^+ of the polymer can act as a reducing agent.[24] This may reduce any previously unreduced chloroaurate ions present in the gold seed solution, especially when an excess of this solution is added to LN@BPEI. The hydrodynamic diameter of LN/Au NPs tends to decrease with the increasing amount of gold on the surface of LN, which is consistent with the increase in the absolute value of their zeta potential from positive in the case of LN@BPEI to highly negative for LN/Au3. This could be attributed to a higher degree of surface coverage by Au seeds for LN/Au3 compared to LN/Au1 and LN/Au2. In fact, the zeta potential value of LN/Au1 is still positive, perhaps due to the predominance of positive charges from BPEI, which negative AuSeeds are unable to screen. As reflected from **Figure S1A**, the coating of LN@BPEI NPs with AuSeeds at the lowest concentration is uneven. However, when the AuSeeds surface density increases, zeta potential becomes negative. This suggests that the AuSeeds negative charge screened the amine groups' positive charge. The gold loading on LN NPs was also verified by EDS (**Figure S2A**), which confirmed increasing gold loading by varying the volume of AuSeeds suspension added to LN@BPEI (**Figure S2A, insert**). This was also supported by previously published XPS analysis.[25] This work showed that upon BPEI coating followed by gold decoration, the presence of Au is

observed in addition to an increase of C and N percentages, while Nb and O percentages decreased. It was also noticed that the Au to Nb atomic ratio increased when the gold seeds to LN ratio increased, as expected. We further confirmed the presence of AuSeeds onto LN@BPEI NPs by STEM and EDS chemical mappings (**Figure 1E3**).

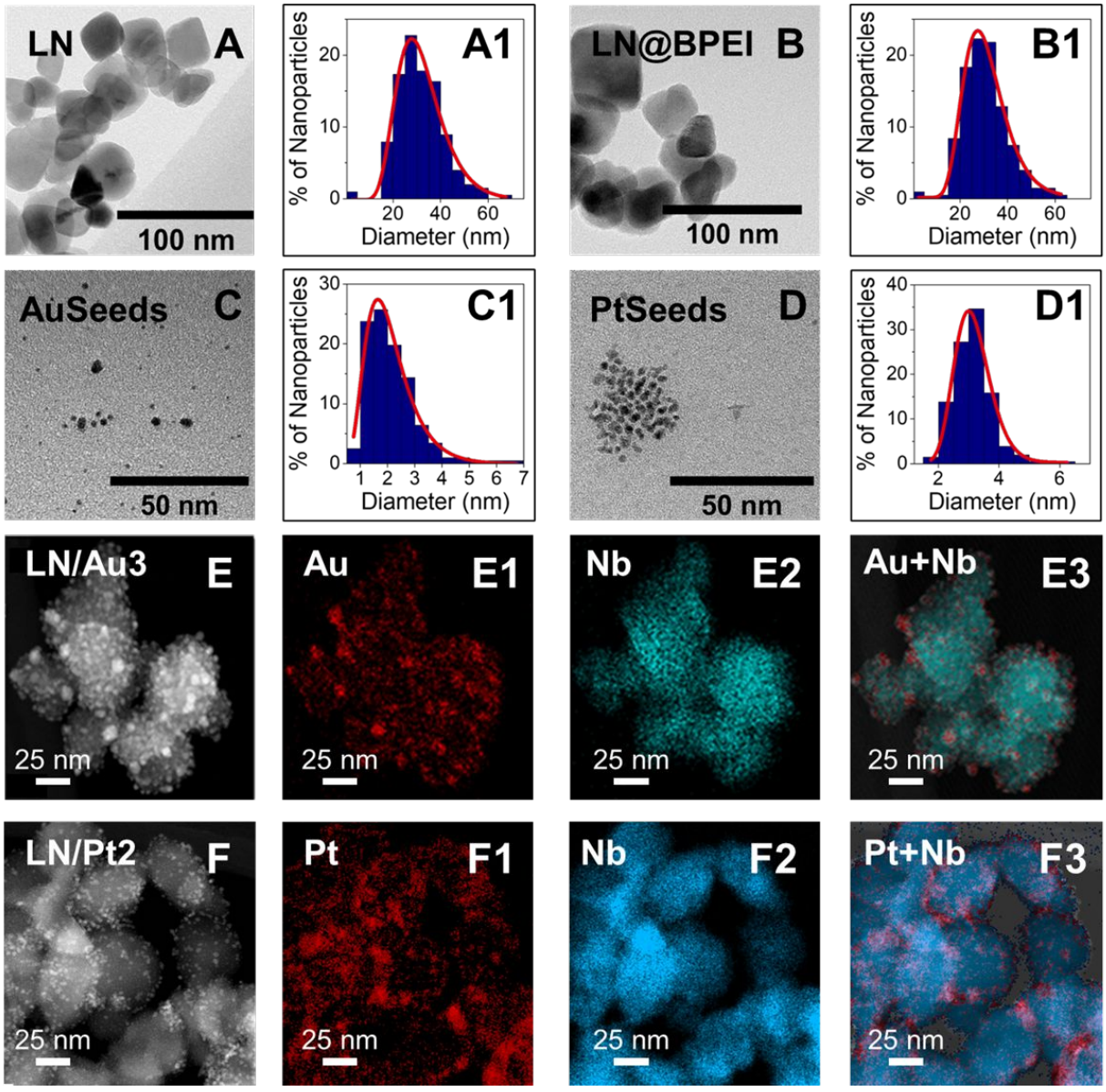

Figure 1. TEM image and TEM size lognormal distribution of (A, A1) LN NPs, (B, B1) LN@BPEI, (C, C1) AuSeeds and (D, D1) PtSeeds. (E) STEM image of LN/Au3 with corresponding EDS chemical maps of (E1) Au, (E2) Nb and (E3) Au and Nb merged on the same image. (F) STEM image of LN/Pt2 with corresponding EDS chemical maps of (F1) Pt, (F2) Nb and (F3) Pt and Nb merged on the same image.

A similar strategy was used to control the surface density of PtSeeds to LN NPs to synthesize LN/Pt. In this case, the particle size calculated from TEM images indicated a slight decrease in the diameter of the PtSeeds. However, changing the concentration does not significantly increase the diameter. In contrast to that observed for LN/Au, the hydrodynamic diameter increased with an increasing amount of Pt on the surface of LN. As shown in **Figure S1E**, the addition of a higher PtSeeds to LN ratio leads to a higher surface density associated with a more homogeneous spatial distribution of PtSeeds onto LN. The zeta potential of LN/Pt NPs decreases with the Pt coverage, starting from a positive value for the lowest Pt amount. For the highest Pt loading, the zeta potential around −12 mV can be associated with low repulsive electrical charges between NPs. This also explains the increase in the hydrodynamic diameter. EDS results show an increasing content of Pt as the ratio of PtSeeds volume to LN@BPEI volume is increased (**Figure S2B, insert**). This was

also confirmed using STEM and EDS chemical mappings (**Figure 1F3**). The batch-to-batch variability in the synthesis and the long-term storage (more than one year) stability of LN/Au and LN/Pt NPs were also assessed. The results are detailed in **Supporting Information** (**Table S2**, **Figures S3 and S4**).

Based on these characterization techniques, we believe that the optimal surface coverage of AuSeeds and PtSeeds could be achieved at the highest concentration *i.e.*, LN/Au3 and LN/Pt2. Additional characterization using HRTEM was performed to gain some understanding of which crystalline facets from AuSeeds and PtSeeds bind to LN and ICP-AES to calculate the concentration of Au, Pt and Nb in each sample. HRTEM images of LN/Au3 (**Figure S6A, Supporting Information**) and PtSeeds in LN/Pt2 (**Figure S6B, Supporting Information**) showed that the same facets of Au and Pt from the cubic fcc crystal structure are on the LN surface, which suggests that similar mode of interactions are likely to be involved during the construction of LN/Au and LN/Pt hybrid materials. ICP-AES measurements revealed that for LN/Au, the Au content of 12.9 % was observed, which corresponds to 40 AuSeeds per LN NP, while for LN/Pt, a Pt content of 16.1 % was observed, which corresponds to 73 PtSeeds per LN NP (detailed calculation is provided in Supporting Information). For further nanozyme experiments, LN/Au3

and LN/Pt2 were selected as they show similar characteristics in terms of an even distribution of the metal seeds on the surface of LN@BPEI.

3.3 Optimization of peroxidase-mimic nanozyme activity of LN/Au NPs and LN/Pt NPs

The catalytic activity optimization was then carried out through absorbance measurements at 650 nm (for ease of understanding, LN/Au3 will be labelled as LN/Au and LN/Pt2 will be labelled as LN/Pt).

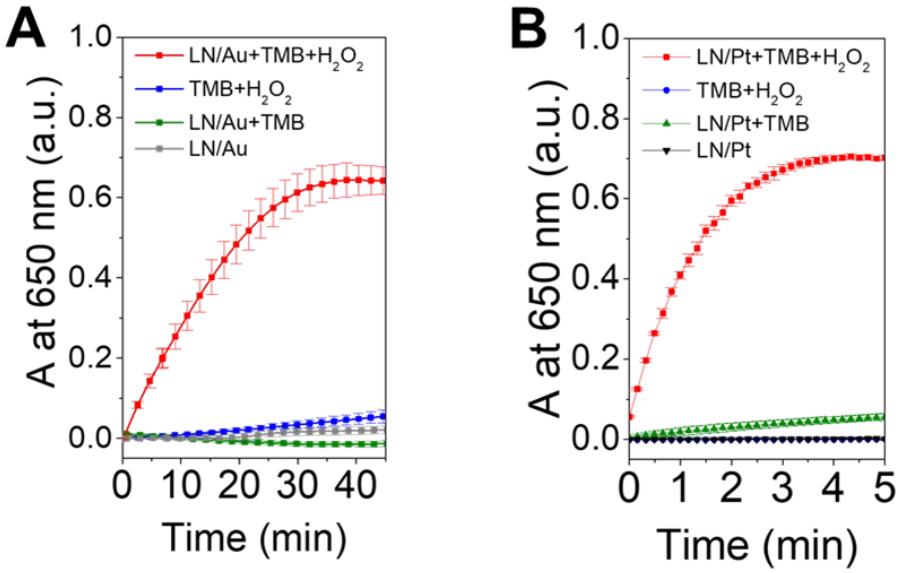

Figure 2. (A) Time-dependent kinetics of the LN/Au nanozyme mediated oxidation of TMB. TMB + LN/Au allowed to test the oxidase activity, TMB + H_2O_2 and LN/Au were negative controls. (B) Time-dependent kinetics of the LN/Pt nanozyme mediated oxidation of TMB. TMB + LN/Pt allowed to test the oxidase activity, TMB + H_2O_2 and LN/Pt were negative controls. TMB and

H_2O_2 concentrations were 167 μM and 29.7 mM, respectively. All the experiments were performed at pH 4 and 37 °C. Y-axis, A is the abbreviation of absorbance.

The first step was to establish the inherent peroxidase-mimic catalytic nanozyme activity of LN/Au. For this, we carried out a time-dependent kinetic study with a fixed amount of LN/Au ([Au] = 27 μM; [$LiNbO_3$] = 182 μM). As seen in **Figure 2A**, the LN/Au nanozyme promotes the oxidation of peroxidase substrate TMB (167 μM) in the presence of H_2O_2 (29.7 mM) as a co-substrate. This is evident from the increase in the absorbance at 650 nm which is due to the oxidation of TMB to its blue-coloured charge transfer product (**Figure S7**). Another important observation was that the LN/Au nanozyme could also promote the catalytic reaction to form the double oxidized yellow coloured diimine product (**Figure S7**). At the 38 min time point, the absorbance corresponding to diimine is less than 10% compared to the one corresponding to the blue complex, which is in agreement with previous works (**Figure S5A**).[5,26] The oxidation of TMB proceeds almost linearly until the saturation point of absorbance, which is obtained after 38 min. However, the reaction does not occur in the absence of H_2O_2, which excludes the oxidase mimic characteristic of these nanozymes.[27–30] We notice negative absorbance values for LN/Au + TMB (green curve) in **Figure 2A**. A possible explanation for this would be the potential aggregation of

LN/Au in the presence of TMB. In the absence of TMB, LN/Au does not seem to aggregate (grey curve) as reflected by the almost constant absorbance. We note that while the y-axis is typically denoted as 'absorbance' in these assays, it is in fact 'extinction' that contains some degree of 'scattering' from the particles (Extinction = Absorption + Scattering). The aggregated particles at higher time points perhaps undergo a lesser degree of scattering than the original well-dispersed particles, or due to aggregation, the effective nanoparticle concentration in the solution reduces. These factors may lead to negative absorbance observed in the green curve. Control experiments performed in the absence of the nanozyme showed insignificant oxidation. This suggests that the peroxidase-mimic activity is an inherent property of LN/Au.

To ascertain that TMB is the optimal substrate for the nanozymes, we exposed the LN/Au nanozyme ([Au] = 27 μM; [$LiNbO_3$] = 182 μM from LN/Au) to a fixed concentration of other commonly used peroxidase substrates (167 μM of ABTS, OPD and TMB) in the presence of H_2O_2 (29.7 mM). As seen in **Figure S8B**, the LN/Au nanozyme promotes the oxidation of all substrates to produce yellow (λ_{max} = 415 nm for OPD), green (λ_{max} = 450 nm for ABTS) and blue (λ_{max} = 650 nm for TMB). Based on the result, TMB was the most optimal substrate, which could be due to favorable interaction between the negatively-charged nanozyme and the positively-charged TMB

[31] and/or the better capability of the nanozyme to detach the oxidized product.[32] Due to its better activity, further studies were performed with TMB as the colorimetric substrate.

We then performed similar experiments to determine the peroxidase-mimic activity of LN/Pt. Considering that Pt is catalytically more active than Au for TMB oxidation as outlined in previous reports [33,34], we optimized the quantity of LN/Pt. For this, we measured the peroxidase mimic activity of LN/Pt at two independent concentrations *viz.*, the same concentration as used for LN/Au (27 μM of Au and 182 μM of LN - 3.9×10^{11} hybrid NPs/mL) and a concentration with ~10 times lower metal content (2.8 μM of Pt and 14.5 μM of LN - 2.8×10^{10} hybrid NPs/mL). Keeping all other reaction conditions consistent ([TMB] = 167 μM, [H_2O_2] = 29.7 μM, pH 4 and 37 °C), both tested concentrations result in TMB oxidation within 5 min (**Figure S9A**). We, therefore, chose the lower concentration of LN/Pt for further experiments. As shown in **Figure 2B**, the time-dependent kinetic study performed using a fixed concentration of LN/Pt ([Pt] = 2.8 μM; [$LiNbO_3$] = 14.5 μM), TMB (167 μM) and H_2O_2 (29.7 mM) showed that the reaction proceeds almost linearly and achieves saturation in less than 5 min (4 min 20s). This means that compared to LN/Au, LN/Pt can complete the reaction 8 times faster using 10 times less metal concentration. This corroborates well with previous reports where Pt is catalytically more active than Au for TMB oxidation for

non-supported Au NPs and Pt NPs and NPs supported on oxides.[33,34] In contrast to LN/Au, LN/Pt was able to promote the oxidation of TMB in the absence of H_2O_2, albeit much more slowly. This suggests that LN/Pt also has some level of oxidase activity. Similar to LN/Au control experiment, the reaction does not proceed in the absence of the nanozyme, confirming that the nanozyme activity is an inherent property of the LN/Pt NPs. Additionally, some level of subsequent oxidation of TMB to yellow diimine product was also observed, similar to LN/Au nanozyme (**Figure S9B**). Based on these results, LN/Pt exhibited higher peroxidase nanozyme activity than LN/Au. The batch-to-batch variability and the long-term storage (more than one year) effect on peroxidase activity were also assessed. The results are detailed in **Supporting Information** (**Figure S5**).

We then optimized the reaction conditions for the peroxidase mimic activity of both nanozymes as a function of pH and temperature (**Figure S10**). Both nanozymes showed activity across a wide temperature range (**Figures S10A and S10C**). In the case of LN/Au nanozyme, optimum peroxidase activity was obtained at 37 °C. The catalytic activity was nearly similar at 20 °C, while higher temperature of 45 °C substantially decreased the activity (~45%). In contrast, the LN/Pt nanozyme showed minimal difference in the activity at all temperatures with 37 °C showing optimal performance. For instance, unlike the LN/Au nanozyme, the catalytic activity of the LN/Pt

nanozyme at higher temperature of 45 °C only decreased the activity by 13%. Optimization of the reaction pH showed that both nanozymes were highly active at pH 4. This is possibly because, at this pH one of the amino groups of TMB will be protonated, favouring the electrostatic interaction between the positively-charged TMB and the negatively-charged nanoparticles.[35] In both cases, the absorbance at 650 nm appears to reduce at lower pH of 3 and 2 (**Figures S10B and S10D**). This may not necessarily reflect poor catalytic performance. At highly acidic pH, the blue product tends to rapidly convert to a yellow product,[36] as reflected from the spectra and the photos of the reaction products at different pH provided in **Figure S11**. It should also be noted that the activity of LN/Pt is relatively better than that observed for LN/Au at pH 3 and 2. This suggests that at lower pH, LN/Pt is able to drive a higher conversion of blue TMB product to the yellow product, compared to that driven by LN/Au (**Figure S11B**). These results corroborate well with previous studies.[36–38]

Finally, the possibility of the potential leaching of gold and platinum ions from LN/Au and LN/Pt, respectively, and their role in catalyzing the reaction were studied by incubating the nanozymes for one hour in pH 4 buffer and exposing the supernatant of the reaction after centrifugation to H_2O_2 (29.7 μM) and TMB (167 μM), while keeping all the other parameters constant (Au, Pt, LN, H_2O_2 and TMB concentrations, pH 4 and 37 °C). The results in **Figure S12**

(Supporting Information) provide evidence of minimal catalytic activity of potentially leached metal ions and confirm that the presence of the nanoparticles is crucial for the reaction to proceed in both systems. From these studies, we can conclude that LN/Au and LN/Pt have peroxidase-mimicking activity and they can readily catalyze the reaction between TMB and H_2O_2 to produce a predominantly blue product (λ_{max} = 650 nm, one electron complex diimine-diamine.[39] Both systems produce residual oxidation to diimine (λ_{max} = 450 nm), which can be neglected when the pH is higher than 3. The catalytic activity of LN/Pt hybrid was better than LN/Au hybrid as the former required 10 times lower metal quantity.

3.4 Synergetic effect of AuSeeds and PtSeeds on the surface of LN.

To understand if the potential synergetic effect created by the interface of LN with the catalytic metal seeds in the hybrid nanoparticles, we compared the ability of LN/Au and LN/Pt to oxidize TMB in the presence of H_2O_2 with the individual components of these hybrids (LN, LN@BPEI, AuSeeds and PtSeeds) and a simple physical mixture of these without BPEI (LN + AuSeeds and LN + PtSeeds) (**Figure 3**). During the oxidation of TMB, it can produce two coloured products: a blue charge transfer complex that results from the combination of TMB and a radical cation initially produced from TMB oxidation and a yellow diimine that results from subsequent

oxidation of radical cation and gives an absorbance maximum at 450 nm (**Figure S7, Supporting Information**).[39] To obtain a more detailed understanding of catalytic performance, the absorbance of the blue oxidized TMB product was measured, and its concentration was calculated using the value of its extinction molar coefficient, i.e. 39000 $L \cdot mol^{-1} \cdot cm^{-1}$ at 650 nm.[29]

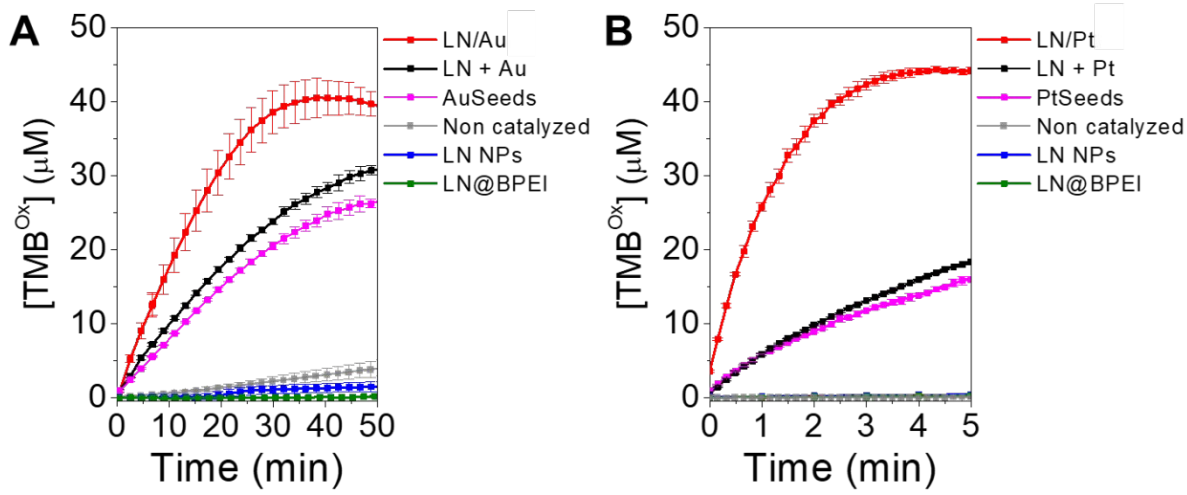

Figure 3. (A) The peroxidase-mimic activity of LN/Au (red) compared to its individual constituents. The concentration of the nanozymes is: [Au] = 27 μM; [$LiNbO_3$] = 182 μM, corresponding to 3.9×10^{11} NPs/mL and 40 AuSeeds per LN. (B) The peroxidase-mimic activity of LN/Pt (red) compared to its individual constituents. The concentration of the nanozymes are: [Pt] = 2.8 μM; [$LiNbO_3$] = 14.5 μM, corresponding to 2.8×10^{10} hybrid NPs/mL and 73 PtSeeds per LN in the reaction well. For both LN/Au and LN/Pt, the measurements were performed in the presence of TMB (167 μM) and H_2O_2 (29.7 mM) at pH 4 and 37˚C.

It is clear that the catalytic activities of LN/Au and LN/Pt are significantly higher than for any other tested component. LN NPs alone do not present any intrinsic peroxidase-like activity, and it may even be the case that they perhaps inhibit the spontaneous basal level oxidation of TMB in the presence of H_2O_2. This observation is even more pronounced for LN@BPEI NPs. To our knowledge, LN has never been reported as a peroxidase-mimic material, although it is well known that LN nanoparticles have photocatalytic and pyro-electrocatalytic applications due to surface charge carrier separation under light excitation or heating.[40] As expected, AuSeeds and PtSeeds have peroxidase-mimicking activities. Noble metal nanoparticles have been extensively studied over the past decade for their peroxidase-like activity,[3] which is affected by several parameters, including their size and surface charge. In particular, ultra-small nanoparticles (diameter below 5 nm) present higher peroxidase activity due to increased surface atoms and therefore an increase of active catalytic sites, which justifies our choice to use 2 nm AuSeeds and PtSeeds. Only a slight increase in their activity is observed when LN NPs are also present in the reaction as a physical mixture. But the overall activity of these physical mixtures remains significantly lower in comparison to LN/Au and LN/Pt hybrid NPs. This suggests that the chemical link created by BPEI between LN NPs and AuSeeds or PtSeeds is necessary to increase the catalytic activity. It has been

reported that metal NPs supported oxides show enhanced catalytic activity.[41–44] A possible mechanism is a charge transfer between the oxide and the metal, increasing the electron density around the junction and thus favouring the electron transfer in redox-type reactions.[45,46] Moreover, the inclusion of the metal onto the oxide surface causes the partial reduction of the latter at the interface, which may potentially create oxygen vacancies. These oxygen-deficient locations within the oxide can help oxygen-containing species (like H_2O_2) to bind and cleave more efficiently and thus enhance the catalytic activity of the hybrid systems.[47,48] The effect of BPEI on peroxidase activity was also investigated using mixtures of metal Seeds with BPEI (Supporting Information). It showed that BPEI plays a significant role when combined with metal Seeds. Indeed, AuSeeds with BPEI presented a slightly higher activity than AuSeeds while PtSeeds with BPEI had a significantly lower activity than PtSeeds. Nevertheless, as shown in **Figures S14C** and **S14D**, respectively, the peroxidase activities of LN/Au and LN/Pt hybrid NPs were still significantly higher than the one metal Seeds and metal Seeds with BPEI, which confirms the synergetic catalytic effect provided by the combination of metal Seeds to LN core. Finally, the dispersion of AuSeeds onto the LN@BPEI surface can also hinder their aggregation during catalysis compared to the pristine form of metal seeds, enhancing the accessibility to the catalytically-active metal

surface, which is key to obtaining better catalytic performance.[49] The combination of these processes is expected to lead to the observed synergetic effect of the enhanced peroxidase-mimic activity of LN/Au and LN/Pt hybrids.

3.5 Calculation of the enzymatic kinetic parameters

As the nanoparticles mimic the activity of natural enzymes, their catalytic parameters can be calculated using the Michaelis-Menten model (**Equation 1**).[3,50] This model allows us to obtain the steady-state kinetics such as maximum velocity (V_{max}), Michaelis constant (K_m), catalytic constant or turnover number (K_{cat}) and catalytic efficiency (K_{eff}). V_{max} is the maximum velocity of catalysis achieved by the system at saturated substrate concentration, and it is directly proportional to the reaction speed. Substrate concentration ([S]) at which the reaction speed is half of the V_{max} is defined by K_m and is inversely proportional to the affinity of the nanozyme towards the substrate (TMB or H_2O_2), i.e., lower the K_m, higher the affinity of the substrate to the nanozyme. K_{cat} indicates the number of molecules converted per unit of time per unit of an enzyme, which can be calculated by dividing V_{max} by the concentration of the enzyme. Although this value permits us to address many mechanism questions, to standardize our data, we need to calculate the K_{eff}, which results from the ratio K_{cat}/K_m. As TMB and H_2O_2 are both substrates for the hybrids, to calculate

these parameters, we varied the concentration of one substrate while keeping the concentration of the other constant.[51] The rest of the parameters were kept constant (pH 4, 37 °C) and nanozyme concentration was fixed for LN/Au ([Au]= 27 μM, [$LiNbO_3$]=182 μM) and LN/Pt ([Pt]=2.8 μM, [$LiNbO_3$]=14.5 μM) (**Figure S15**). We also calculated the steady state kinetic parameters for AuSeeds and PtSeeds and compared them to the hybrid nanozymes (**Table S4**). It has to be pointed out that to calculate K_{cat}, V_{max} is divided by the concentration of enzyme, which in this case is nanozyme. We considered that AuSeeds and PtSeeds were the catalytic hot points in LN/Au and LN/Pt and that each surface metal atom works as a single enzyme (detailed calculation is provided in **Supporting Information**).[52] LN NPs were not considered in this calculation as they did not show any peroxidase mimics (**Figure 3**). We note that the calculated values of kinetic parameters, in particular K_{cat} will depend upon the consideration of whether a single metal atom or a single metal nanoparticle is considered equivalent to a single nanozyme. Since the surface atoms of metal NPs are expected to predominantly participate in the catalysis reaction, it can be safely presumed that a single metal NP will offer more than one catalytic site, while at the same time, all atoms (particularly those not on the NP surface) will not participate in catalysis. Since it is highly challenging to determine the absolute number of catalytic sites on a particle, we employed the

number of surface metal atoms available during the reaction, as this will underestimate the catalytic efficiency, rather than reporting an overestimated efficiency. Overall, irrespective of the calculated values, the relative values among the different samples are still valid and can be confidently compared.

Equation 1. Michaelis-Menten natural enzyme model.

$$V = \frac{V_{max}[S]}{K_M + [S]}$$

From the data presented in **Table S4**, it is clear that all the nanozymes show a higher affinity for TMB over H_2O_2. This suggests a preference of these nanozymes towards TMB adsorption over H_2O_2. If we compare the K_m of the hybrid with the respective metal seed, the affinity towards H_2O_2 improves while the affinity towards TMB decreases in the hybrids. The higher affinity to H_2O_2 could be attributed to the creation of oxygen vacancies at the LN/metal interface.[50,53] On the other hand, the decrease in the affinity for TMB can be due to the steric hindrance caused by BPEI on their surface and the larger size of TMB that may impede its interaction with the hybrid.[35] Further, while Au-containing nanozymes have a higher affinity to TMB, the Pt-containing nanozymes have a higher affinity to H_2O_2. This is consistent with previous observations in the literature.[3,33] In the context of V_{max}, the LN/metal hybrids can drive the reaction faster than their corresponding metal

seeds, particularly in the case of Pt system, where ~15-20 times increase in the reaction velocity is observed.

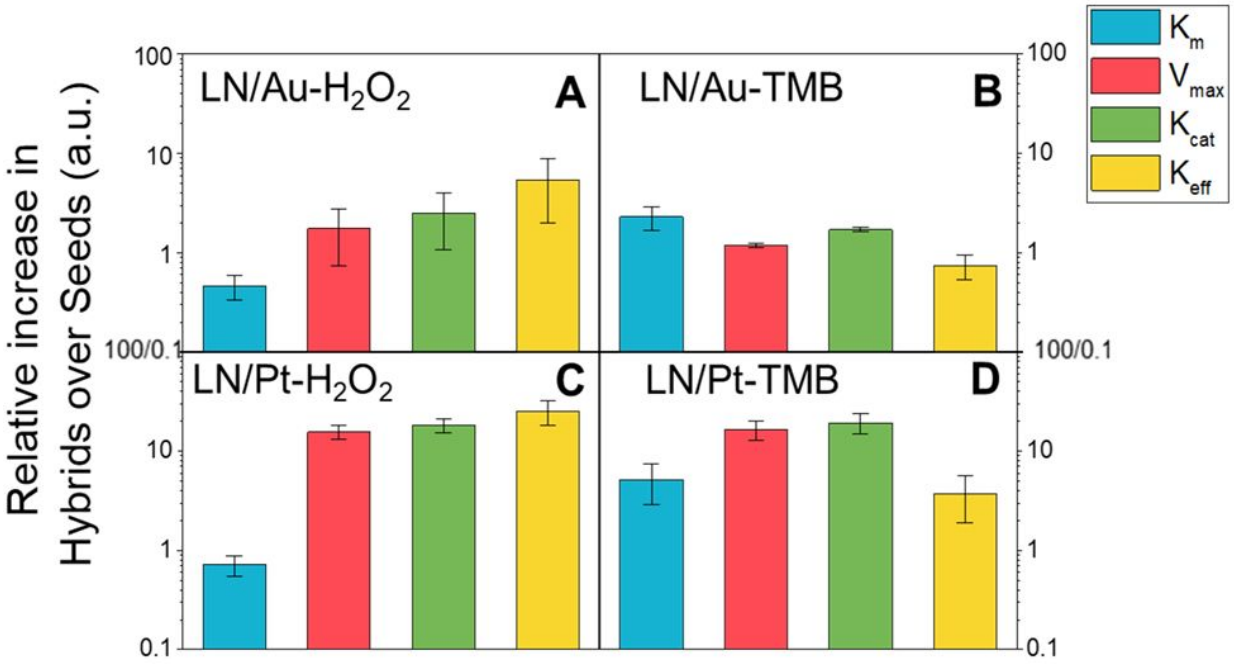

Figure 4. Relative increase of steady kinetic parameters calculated from the number of surface metal atoms of hybrids over seeds. LN/Au increase over AuSeeds with H_2O_2 as a substrate (A). LN/Au3 increase over AuSeeds with TMB as a substrate (B). LN/Pt increase over PtSeeds with H_2O_2 as a substrate (C). LN/Pt increase over PtSeeds with TMB as a substrate (D).

The relative increase in the K_{cat} and K_{eff} of the hybrid nanozymes for H_2O_2 was much more pronounced than that observed for the metal seeds (**Figure 4**). This increase was 18-25 times higher in the case of the LN/Pt hybrids (**Figure 4C**) and 2.5-5 times higher in LN/Au hybrids (**Figure 4A**)

supporting the synergetic effect provided by the interface between LN and metal NPs. A comparison between the hybrids showed that the K_{cat} and K_{eff} for LN/Pt hybrids were more noticeable than LN/Au hybrids. This increase in the K_{cat} and K_{eff} for LN/Pt hybrids may be due to the stronger affinity of H_2O_2 to Pt NPs (lower K_m for H_2O_2), which will allow for efficient cleavage of H_2O_2 to produce $^{\bullet}OH$ radicals. When we compared the K_{cat} and K_{eff} of the hybrid nanozymes for TMB, the increase was not as pronounced as that observed for H_2O_2. This suggests that the catalytic efficiency for TMB oxidation is lower than that for H_2O_2.

A combination of a favourable K_m and V_{max} obtained for the hybrid nanozymes translates into a higher K_{cat} and K_{eff} for the hybrids over pristine metal seeds, specifically for H_2O_2. In the case of TMB, the K_{cat} for both hybrids is higher than the metal seeds (**Figure 4B and 4D**). This is not surprising as this parameter depends on the surface atoms, which remains consistent over the reaction. However, the K_{eff} for TMB decreases unlike the observation in the case of H_2O_2. This is due to the higher affinity of the AuSeeds and PtSeeds for TMB than the hybrids (**Table S4**). Even though the relative increase in the K_{eff} is lower for the hybrids over the respective seeds, the catalytic reaction is considerably faster for LN/Au and LN/Pt.

We can state that the hybrid nanozymes present the best performance compared to the pristine metal seeds for the H_2O_2 substrate. This improvement has exciting potential applications in biomedicine. For instance, both LN/Au and LN/Pt nanozymes show low K_m and high V_{max} values for H_2O_2 (**Table S4**, **Supporting Information**), which are required for sensing applications.[54] This would allow us to detect H_2O_2 in biological samples in the mM range. The antimicrobial effect of nanozymes would also benefit from these improved enzymatic properties for H_2O_2. It is commonly admitted that peroxidase mimics in metal and metal oxide nanozymes produce reactive oxygen species (ROS), specially HO·.[3] These extremely oxidative species are widely used as antimicrobial agents.[55] Indeed, the higher affinity towards H_2O_2 implies a lower H_2O_2 concentration needed to produce HO·. In addition, the higher V_{max} values (for H_2O_2 substrate) obtained for LN/Au and LN/Pt (**Table S4**, **Supporting Information**) suggest that the production of HO· radicals would be over around 1.5-fold and 11-fold faster than for the pristine nanoparticles, respectively. This would enhance the antimicrobial effect for LN/Au and moreover for LN/Pt.

Many other studies report the kinetic parameters of hybrid nanozymes combining metal and metal oxide.[56–58] However, the calculation of K_{cat} and K_{eff}, which gives a better comprehension of the nanozyme's performance, is either missing or calculated considering that each nanoparticle is

a catalytic site, thus overestimating the performance of the nanozyme. Here we used the calculation method provided by Zandieh et al in which each surface metal atom is a catalytic site.[59] **Table 3** presents K_{cat} and K_{eff} values for LN/Au and LN/Pt compared to the values obtained for 300 nm Fe_3O_4 nanozymes, which were calculated based on the number of surface Fe atoms, and for the natural enzyme, horseradish peroxidase (HRP).[60]

Table 3. Comparison of LN/Au and LN/Pt efficiency constants for TMB and H_2O_2 with Fe_3O_4 nanozyme (300 nm) and horseradish peroxidase.

Nanozyme	**H_2O_2 K_{eff} ($M^{-1}\cdot s^{-1}$)**	**TMB K_{eff} ($M^{-1}\cdot s^{-1}$)**	**Reference**
LN/Au	0.26	128.8	This work
LN/Pt	64	5.0×10^3	This work
Fe_3O_4 (300 nm)	0.38	210	[60]
HRP	9.5×10^5	9.2×10^6	[60]

The above results (**Table 3**) show that LN/Au and Fe_3O_4 nanozymes present similar levels of efficiency. However, LN/Pt nanozymes overcome the efficiency of Fe_3O_4 by 2 and 1 orders of magnitude for H_2O_2 and TMB substrates, respectively. The presence of oxygen vacancies created

on the surface of $LiNbO_3$ due to the presence of PtSeeds may increase the affinity towards H_2O_2. However, the nanozymes presented in **Table 3** do not overcome the performance of natural enzyme HRP that surpasses by 4 and 3 orders of magnitude the performance of LN/Pt for H_2O_2 and TMB substrates, respectively, suggesting that there is still room for improving the efficiency of nanozymes. Nevertheless, nanozymes present other advantages, for instance, stability over time, resistance towards harsh conditions or easiness of fabrication, which make them interesting for biomedical applications.[1]

4 Conclusions

In summary, we have created hybrid nanoparticles combining $LiNbO_3$ NPs with AuSeeds and PtSeeds using layer-by-layer synthesis introducing BPEI as a linker. The metal loading in the hybrid LN/Au and LN/Pt nanoparticles was controlled by varying the ratio of the volume ratio between metal seeds dispersion to LN@BPEI dispersion. The hybrids with the optimal surface coverage of the metal seeds showed that ~40 AuSeeds were associated per LN, while ~70 PtSeeds were associated per LN. These hybrids showed catalytic activity similar to natural peroxidase enzymes. The nanozyme activity of the LN/Pt hybrid was 8 times faster than LN/Au hybrids even with 10 times lower Pt concentration suggesting that LN/Pt is a faster and more powerful

nanozyme than LN/Au. We also observed that the catalytic activity of the hybrid nanozymes was higher than the individual counterparts or a simple mixture containing a similar concentration of the individual counterparts. The affinity of the hybrids to H_2O_2 improved while decreasing for TMB when compared to the respective metal seeds. However, the V_{max} for both TMB and H_2O_2 showed improvement when compared to the respective metal seeds. Based on this study, the interface between the LN NPs and the Au or PtSeeds is critical to achieve superior catalytic activity. This ability to achieve superior nanozyme activity can be employed in a variety of applications such as sensing, biomedicine or environmental treatment. Their low K_m and high V_{max} values would thus make them appropriate for H_2O_2 sensing or antimicrobial agents.

ASSOCIATED CONTENT

Supporting Information. Materials and methods, TEM images and size distribution of seeds of hybrid nanoparticles, EDS characterization of hybrid nanoparticles, batch-to-batch reproducibility and long-term stability, HRTEM images and facets of metal seeds of LN/Au3 and LN/Pt2, number of nanoparticles calculation and metal surface atoms calculation, TMB oxidation pathway and spectra at pH 4, optimization of peroxidase mimics for LN/Au and LN/Pt, temperature and pH

optimization for LN/Au and LN/Pt, ions leaching test, effect of BPEI on the peroxidase-mimic activity and Michaelis-Menten curve fitting and parameters. The following files are available free of charge (PDF).

AUTHOR INFORMATION

Corresponding Author

*Virginie Monnier – Univ Lyon, Ecole Centrale de Lyon, CNRS, INSA Lyon, Université Claude Bernard Lyon 1, CPE Lyon, INL, UMR5270, 69130 Ecully, France.

Authors

Ana-María Pablo-Sainz-Ezquerra – Univ Lyon, Ecole Centrale de Lyon, CNRS, INSA Lyon, Université Claude Bernard Lyon 1, CPE Lyon, INL, UMR5270, 69130 Ecully, France and Sir Ian Potter NanoBioSensing Facility, NanoBiotechnology Research Laboratory, RMIT University, Melbourne, Victoria, 3000, Australia.

Rachael Taitt – Univ Lyon, Ecole Centrale de Lyon, CNRS, INSA Lyon, Université Claude Bernard Lyon 1, CPE Lyon, INL, UMR5270, 69130 Ecully, France.

Florian Riporto – Université Savoie Mont Blanc, SYMME, F-74000 Annecy, France.

Yannick Mugnier – Université Savoie Mont Blanc, SYMME, F-74000 Annecy, France.

Pyria Rose Divina Mariathomas – Sir Ian Potter NanoBioSensing Facility, NanoBiotechnology Research Laboratory, RMIT University, Melbourne, Victoria, 3000, Australia.

Ronan Le Dantec – Université Savoie Mont Blanc, SYMME, F-74000 Annecy, France.

Mimoun Aouine – Univ Lyon, Université Claude Bernard Lyon 1, CNRS, IRCELYON, Villeurbanne, F-69626, France.

Christophe Geantet – Univ Lyon, Université Claude Bernard Lyon 1, CNRS, IRCELYON, Villeurbanne, F-69626, France.

Rajesh Ramanathan – Sir Ian Potter NanoBioSensing Facility, NanoBiotechnology Research Laboratory, RMIT University, Melbourne, Victoria, 3000, Australia.

Vipul Bansal – Sir Ian Potter NanoBioSensing Facility, NanoBiotechnology Research Laboratory, RMIT University, Melbourne, Victoria, 3000, Australia.

Yann Chevolot – Univ Lyon, CNRS, INSA Lyon, Ecole Centrale de Lyon, Université Claude Bernard Lyon 1, CPE Lyon, INL, UMR5270, 69130 Ecully, France.

Author Contributions

A.M.P.S.E. carried out the experiments. A.M.P.S.E. wrote the manuscript with support from V.M., Y.C., V.B.R.R., F.R., Y.M. and R.D. fabricated the LN NPs sample. P.R.D.M helped A.M.P.S.E. implementing the peroxidase-mimics experiments. Correction and review were performed by all authors. All authors have given approval to the final version of the manuscript.

Funding Sources

This research was primarily funded by the ECLAUsion program. The ECLAUSion project has received funding from the European Union's Horizon 2020 research and innovation programme under the Marie Skłodowska-Curie grant agreement No 801512. We acknowledge the support of the International Associated Laboratory in Photonics between France and Australia (LIA ALPhFA). V. Bansal and R. Ramanathan acknowledge the Australian Research Council (ARC) for funding support through the Discovery Grant No. DP230101650.

Notes

Any additional relevant notes should be placed here.

ACKNOWLEDGEMENTS

This research was primarily funded by the ECLAUsion program. The ECLAUSion project has received funding from the European Union's Horizon 2020 research and innovation programme under the Marie Skłodowska-Curie grant agreement No 801512. We acknowledge the support of the International Associated Laboratory in Photonics between France and Australia (LIA ALPhFA). V. Bansal and R. Ramanathan acknowledge the Australian Research Council for research support through an ARC Discovery (DP230101650) grant. V. Bansal acknowledges the Ian Potter Foundation for establishing the Sir Ian Potter NanoBioSensing Facility at RMIT University. N. Blanchard and the Centre Lyonnais de Microscopie (CLYM) platform are thanked for their help with TEM experiments. We are grateful to R. Rieger and H. Zahouani for the access to the IVTV platform, where we performed well-plate reader experiments. Thanks are given to the NanoLyon platform for technical support.

ABBREVIATIONS

LN, $LiNbO_3$; NP, nanoparticle; BPEI, branched polyethyleneimine; TMB, 3,3',5,5'-tetramethylbenzidine; LN/Au, $LiNbO_3$ NPs coated with BPEI and AuSeeds; LN/Pt, $LiNbO_3$ NPs coated with BPEI and PtSeeds.

REFERENCES

(1) Huang, Y.; Ren, J.; Qu, X. Nanozymes: Classification, Catalytic Mechanisms, Activity Regulation, and Applications. *Chem. Rev.* **2019**, *119* (6), 4357–4412. https://doi.org/10.1021/acs.chemrev.8b00672.

(2) Naveen Prasad, S.; Bansal, V.; Ramanathan, R. Detection of Pesticides Using Nanozymes: Trends, Challenges and Outlook. *TrAC - Trends Anal. Chem.* **2021**, *144*, 116429. https://doi.org/10.1016/j.trac.2021.116429.

(3) Yan, X.; Gao, L. *Nanozymology*; Yan, X., Ed.; Springer: Singapore, 2020. https://doi.org/10.1007/978-981-15-1490-6.

(4) Mohapatra, A.; Uthaman, S.; Park, I. K. External and Internal Stimuli-Responsive Metallic Nanotherapeutics for Enhanced Anticancer Therapy. *Front. Mol. Biosci.* **2021**, *7* (January), 1–32. https://doi.org/10.3389/fmolb.2020.597634.

(5) Sun, X.; Guo, S.; Chung, C.-S. S.; Zhu, W.; Sun, S. A Sensitive H_2O_2 Assay Based on Dumbbell-like PtPd-Fe_3O_4 Nanoparticles. *Adv. Mater.* **2013**, *25* (1), 132–136. https://doi.org/10.1002/adma.201203218.

(6) Naveen Prasad, S.; Anderson, S. R.; Joglekar, M. V.; Hardikar, A. A.; Bansal, V.; Ramanathan, R. Bimetallic Nanozyme Mediated Urine Glucose Monitoring through Discriminant Analysis of Colorimetric Signal. *Biosens. Bioelectron.* **2022**, *212* (April), 114386. https://doi.org/10.1016/j.bios.2022.114386.

(7) Lee, Y.; Garcia, M. A.; Frey Huls, N. A.; Sun, S. Synthetic Tuning of the Catalytic Properties of Au-Fe_3O_4 Nanoparticles. *Angew. Chemie Int. Ed.* **2010**, *49* (7), 1271–1274. https://doi.org/10.1002/anie.200906130.

(8) Mohanty, D.; Chaubey, G. S.; Yourdkhani, A.; Adireddy, S.; Caruntu, G.; Wiley, J. B. Synthesis and Piezoelectric Response of Cubic and Spherical $LiNbO_3$ Nanocrystals. *RSC Adv.* **2012**, *2* (5), 1913. https://doi.org/10.1039/c2ra00628f.

(9) Fedotova, A.; Carletti, L.; Zilli, A.; Setzpfandt, F.; Staude, I.; Toma, A.; Finazzi, M.; De Angelis, C.; Pertsch, T.; Neshev, D. N.; Celebrano, M. Lithium Niobate Meta-Optics. *ACS Photonics* **2022**, *9*, 3745–3763. https://doi.org/10.1021/acsphotonics.2c00835.

(10) Dantelle, G.; Beauquis, S.; Le Dantec, R.; Monnier, V.; Galez, C.; Mugnier, Y. Solution-Based Synthesis Routes for the Preparation of Noncentrosymmetric 0-D Oxide Nanocrystals with Perovskite and Nonperovskite Structures. *Small* **2022**, *18*, 2200992. https://doi.org/10.1002/smll.202200992.

(11) Vuilleumier, J.; Gaulier, G.; De Matos, R.; Mugnier, Y.; Campargue, G.; Wolf, J.-P.; Bonacina, L.; Gerber-Lemaire, S. Photocontrolled Release of the Anticancer Drug Chlorambucil with Caged Harmonic Nanoparticles. *Helv. Chim. Acta* **2019**, *103*, e1900251. https://doi.org/10.1002/hlca.201900251.

(12) Staedler, D.; Magouroux, T.; Hadji, R.; Joulaud, C.; Extermann, J.; Schwung, S.; Passemard, S.; Kasparian, C.; Clarke, G.; Gerrmann, M.; Dantec, R. Le; Mugnier, Y.; Rytz, D.; Ciepielewski, D.; Galez, C.; Gerber-Lemaire, S.; Juillerat-Jeanneret, L.; Bonacina, L.; Wolf, J. P. Harmonic Nanocrystals for Biolabeling: A Survey of Optical Properties and Biocompatibility. *ACS Nano* **2012**, *6*, 2542–2549. https://doi.org/10.1021/nn204990n.

(13) Khan, M. A.; Nadeem, M. A.; Idriss, H. Ferroelectric Polarization Effect on Surface Chemistry and Photo-Catalytic Activity: A Review. *Surf. Sci. Rep.* **2016**, *71* (1), 1–31. https://doi.org/10.1016/j.surfrep.2016.01.001.

(14) Nath, R. K.; Zain, M. F. M.; Kadhum, A. A. H.; Kaish, A. B. M. A. An Investigation of $LiNbO_3$ Photocatalyst Coating on Concrete Surface for Improving Indoor Air Quality. *Constr. Build. Mater.* **2014**, *54*, 348–353. https://doi.org/10.1016/j.conbuildmat.2013.12.072.

(15) Zhu, X.; Altman, E. I. Surface and Interface Properties of Polar Thin Films on a Ferroelectric Substrate: ZnO on LiNbO 3 (0001) and (000 1^{-}) . *J. Vac. Sci. Technol. A Vacuum, Surfaces, Film.* **2018**, *36* (2), 021511. https://doi.org/10.1116/1.5012762.

(16) Sánchez-Dena, O.; Villalobos-Mendoza, S. D.; Farías, R.; Fierro-Ruiz, C. D. Lithium

Niobate Single Crystals and Powders Reviewed—Part II. *Crystals* **2020**, *10* (11), 1–33. https://doi.org/10.3390/cryst10110990.

(17) Cai, B.; Zhao, M.; Ma, Y.; Ye, Z.; Huang, J. Bio-Inspired Formation of Mesoporous $LiNbO_3$ Nanotubes and Application for Glucose Biosensor. *Electrochim. Acta* **2014**, *147*, 176–182. https://doi.org/10.1016/j.electacta.2014.09.054.

(18) Urbain, M.; Riporto, F.; Beauquis, S.; Monnier, V.; Marty, J. C.; Galez, C.; Durand, C.; Chevolot, Y.; Le Dantec, R.; Mugnier, Y. On the Reaction Pathways and Growth Mechanisms of LiNbO3 Nanocrystals from the Non-Aqueous Solvothermal Alkoxide Route. *Nanomaterials* **2021**, *11* (1), 154. https://doi.org/10.3390/nano11010154.

(19) Taitt, R.; Urbain, M.; Behel, Z.; Pablo-Sainz-Ezquerra, A.-M.; Kandybka, I.; Millet, E.; Martinez-Rodriguez, N.; Yeromonahos, C.; Beauquis, S.; Le Dantec, R.; Mugnier, Y.; Brevet, P.-F.; Chevolot, Y.; Monnier, V. Gold-Seeded Lithium Niobate Nanoparticles : Influence of Gold Surface Coverage on Second Harmonic Properties. *Nanomaterials* **2021**, *11*, 950. https://doi.org/10.3390/nano11040950.

(20) Bryan, W. W.; Jamison, A. C.; Chinwangso, P.; Rittikulsittichai, S.; Lee, T. C.; Lee, T. R. Preparation of THPC-Generated Silver, Platinum, and Palladium Nanoparticles and Their Use in the Synthesis of Ag, Pt, Pd, and Pt/Ag Nanoshells. *RSC Adv.* **2016**, *6* (72), 68150–68159. https://doi.org/10.1039/c6ra10717f.

(21) Bhatt, R.; Bhaumik, I.; Ganesamoorthy, S.; Karnal, A. K.; Swami, M. K.; Patel, H. S.; Gupta, P. K. Urbach Tail and Bandgap Analysis in near Stoichiometric $LiNbO_3$ Crystals. *Phys. Status Solidi Appl. Mater. Sci.* **2012**, *209* (1), 176–180. https://doi.org/10.1002/pssa.201127361.

(22) Curtis, K. A.; Miller, D.; Millard, P.; Basu, S.; Horkay, F.; Chandran, P. L. Unusual Salt and PH Induced Changes in Polyethylenimine Solutions. *PLoS One* **2016**, *11*, e0158147. https://doi.org/10.1371/journal.pone.0158147.

(23) Naguib, Y. W.; Cui, Z. *Nanomedicine: The Promise and Challenges in Cancer Chemotherapy*; Capco, D. G., Chen, Y., Eds.; Advances in Experimental Medicine and

Biology; Springer: Dordrecht, 2014; Vol. 811. https://doi.org/10.1007/978-94-017-8739-0.

(24) Liebig, F.; Sarhan, R. M.; Prietzel, C.; Thünemann, A. F.; Bargheer, M.; Koetz, J. Undulated Gold Nanoplatelet Superstructures: In Situ Growth of Hemispherical Gold Nanoparticles onto the Surface of Gold Nanotriangles. *Langmuir* **2018**, *34* (15), 4584–4594. https://doi.org/10.1021/acs.langmuir.7b02898.

(25) Taitt, R.; Urbain, M.; Bredillet, K.; Behel, Z.; Ceccone, G.; Bañuls-Ciscar, J.; Beauquis, S.; Mugnier, Y.; Brevet, P. F.; Le Dantec, R.; Chevolot, Y.; Monnier, V. Gold Raspberry Shell Grown onto Nonspherical Lithium Niobate Nanoparticles for Second Harmonic Generation and Photothermal Applications. *Part. Part. Syst. Charact.* **2022**, 2200093. https://doi.org/10.1002/ppsc.202200093.

(26) Jv, Y.; Li, B.; Cao, R. Positively-Charged Gold Nanoparticles as Peroxidiase Mimic and Their Application in Hydrogen Peroxide and Glucose Detection. *Chem. Commun.* **2010**, *46* (42), 8017–8019. https://doi.org/10.1039/c0cc02698k.

(27) Singh, M.; Weerathunge, P.; Liyanage, P. D.; Mayes, E.; Ramanathan, R.; Bansal, V. Competitive Inhibition of the Enzyme-Mimic Activity of Gd-Based Nanorods toward Highly Specific Colorimetric Sensing of l -Cysteine. *Langmuir* **2017**, *33* (38), 10006–10015. https://doi.org/10.1021/acs.langmuir.7b01926.

(28) Gao, Z.; Xu, M.; Hou, L.; Chen, G.; Tang, D. Irregular-Shaped Platinum Nanoparticles as Peroxidase Mimics for Highly Efficient Colorimetric Immunoassay. *Anal. Chim. Acta* **2013**, *776*, 79–86. https://doi.org/10.1016/j.aca.2013.03.034.

(29) Weerathunge, P.; Behera, B. K.; Zihara, S.; Singh, M.; Prasad, S. N.; Hashmi, S.; Mariathomas, P. R. D.; Bansal, V.; Ramanathan, R. Dynamic Interactions between Peroxidase-Mimic Silver NanoZymes and Chlorpyrifos-Specific Aptamers Enable Highly-Specific Pesticide Sensing in River Water. *Anal. Chim. Acta* **2019**, *1083*, 157–165. https://doi.org/10.1016/j.aca.2019.07.066.

(30) Gao, L.; Fan, K.; Yan, X. Iron Oxide Nanozyme: A Multifunctional Enzyme Mimetic for Biomedical Applications. *Theranostics* **2017**, *7* (13), 3207–3227.

https://doi.org/10.7150/thno.19738.

(31) Hu, J.; Ni, P.; Dai, H.; Sun, Y.; Wang, Y.; Jiang, S.; Li, Z. A Facile Label-Free Colorimetric Aptasensor for Ricin Based on the Peroxidase-like Activity of Gold Nanoparticles. *RSC Adv.* **2015**, *5* (21), 16036–16041. https://doi.org/10.1039/C4RA17327A.

(32) Walther, R.; Winther, A. K.; Fruergaard, A. S.; van den Akker, W.; Sørensen, L.; Nielsen, S. M.; Jarlstad Olesen, M. T.; Dai, Y.; Jeppesen, H. S.; Lamagni, P.; Savateev, A.; Pedersen, S. L.; Frich, C. K.; Vigier-Carrière, C.; Lock, N.; Singh, M.; Bansal, V.; Meyer, R. L.; Zelikin, A. N. Identification and Directed Development of Non-Organic Catalysts with Apparent Pan-Enzymatic Mimicry into Nanozymes for Efficient Prodrug Conversion. *Angew. Chemie - Int. Ed.* **2019**, *58* (1), 278–282. https://doi.org/10.1002/anie.201812668.

(33) Li, J.; Liu, W.; Wu, X.; Gao, X. Mechanism of PH-Switchable Peroxidase and Catalase-like Activities of Gold, Silver, Platinum and Palladium. *Biomaterials* **2015**, *48*, 37–44. https://doi.org/10.1016/j.biomaterials.2015.01.012.

(34) Xiao, P.; Zhao, Y.; Wang, T.; Zhan, Y.; Wang, H.; Li, J.; Thomas, A.; Zhu, J. Polymeric Carbon Nitride/Mesoporous Silica Composites as Catalyst Support for Au and Pt Nanoparticles. *Chem. - A Eur. J.* **2014**, *20* (10), 2872–2878. https://doi.org/10.1002/chem.201303741.

(35) Moreno-Castilla, C.; Naranjo, Á.; Victoria López-Ramón, M.; Siles, E.; López-Peñalver, J. J.; de Almodóvar, J. M. R. Influence of the Hydrodynamic Size and ζ Potential of Manganese Ferrite Nanozymes as Peroxidase-Mimicking Catalysts at PH 4 in Different Buffers. *J. Catal.* **2022**, *414*, 179–185. https://doi.org/10.1016/j.jcat.2022.09.010.

(36) Drozd, M.; Pietrzak, M.; Parzuchowski, P. G.; Malinowska, E. Pitfalls and Capabilities of Various Hydrogen Donors in Evaluation of Peroxidase-like Activity of Gold Nanoparticles. *Anal. Bioanal. Chem.* **2016**, *408* (29), 8505–8513. https://doi.org/10.1007/s00216-016-9976-z.

(37) Jiang, B.; Duan, D.; Gao, L.; Zhou, M.; Fan, K.; Tang, Y.; Xi, J.; Bi, Y.; Tong, Z.; Gao, G. F.; Xie, N.; Tang, A.; Nie, G.; Liang, M.; Yan, X. Standardized Assays for Determining the

Catalytic Activity and Kinetics of Peroxidase-like Nanozymes. *Nat. Protoc.* **2018**, *13* (7), 1506–1520. https://doi.org/10.1038/s41596-018-0001-1.

(38) Sun, H.; Jiao, X.; Han, Y.; Jiang, Z.; Chen, D. Synthesis of Fe_3O_4-Au Nanocomposites with Enhanced Peroxidase-Like Activity. *Eur. J. Inorg. Chem.* **2013**, *2013* (1), 109–114. https://doi.org/10.1002/ejic.201201159.

(39) Josephy, D.; Eling, T.; Mason, R. The Horseradish Peroxidase-Catalyzed Oxidation of 3,5,3',5'- Tetramethylbenzidine. *J. Biol. Chem.* **1982**, *257* (7), 3669–3675.

(40) Amaechi, I. C.; Hadj Youssef, A.; Dörfler, A.; González, Y.; Katoch, R.; Ruediger, A. Catalytic Applications of Non-Centrosymmetric Oxide Nanomaterials. *Angew. Chemie - Int. Ed.* **2022**, *61* (43), e202207975. https://doi.org/10.1002/anie.202207975.

(41) Haruta, M.; Kobayashi, T.; Sano, H.; Yamada, N. Novel Gold Catalysts for the Oxidation of Carbon Monoxide at a Temperature Far Below 0 °C. *Chem. Lett.* **1987**, *16* (2), 405–408. https://doi.org/10.1246/cl.1987.405.

(42) Schubert, M. M.; Hackenberg, S.; Van Veen, A. C.; Muhler, M.; Plzak, V.; Behm, J. J. CO Oxidation over Supported Gold Catalysts -"Inert" and "Active" Support Materials and Their Role for the Oxygen Supply during Reaction. *J. Catal.* **2001**, *197* (1), 113–122. https://doi.org/10.1006/jcat.2000.3069.

(43) Sun, X.; Guo, S.; Liu, Y.; Sun, S. Dumbbell-like PtPd–Fe_3O_4 Nanoparticles for Enhanced Electrochemical Detection of H_2O_2. *Nano Lett.* **2012**, *12* (9), 4859–4863. https://doi.org/10.1021/nl302358e.

(44) Jońca, J.; Harmel, J.; Joanny, L.; Ryzhikov, A.; Kahn, M. L.; Fau, P.; Chaudret, B.; Fajerwerg, K. Au/MOx (M = Zn, Ti) Nanocomposites as Highly Efficient Catalytic Filters for Chemical Gas Sensing at Room Temperature and in Humid Atmosphere. *Sensors Actuators, B Chem.* **2017**, *249*, 357–363. https://doi.org/10.1016/j.snb.2017.04.061.

(45) Lopes, G.; Vargas, J. M.; Sharma, S. K.; Béron, F.; Pirota, K. R.; Knobel, M.; Rettori, C.; Zysler, R. D. Ag-Fe_3O_4 Dimer Colloidal Nanoparticles: Synthesis and Enhancement of Magnetic Properties. *J. Phys. Chem. C* **2010**, *114* (22), 10148–10152.

https://doi.org/10.1021/jp102311u.

(46) Scanlon, M. D.; Peljo, P.; Méndez, M. A.; Smirnov, E.; Girault, H. H. Charging and Discharging at the Nanoscale: Fermi Level Equilibration of Metallic Nanoparticles. *Chem. Sci.* **2015**, *6* (5), 2705–2720. https://doi.org/10.1039/c5sc00461f.

(47) Delannoy, L.; Fajerwerg, K.; Lakshmanan, P.; Potvin, C.; Méthivier, C.; Louis, C. Supported Gold Catalysts for the Decomposition of VOC: Total Oxidation of Propene in Low Concentration as Model Reaction. *Appl. Catal. B Environ.* **2010**, *94* (1–2), 117–124. https://doi.org/10.1016/j.apcatb.2009.10.028.

(48) Kim, S. M.; Lee, H.; Park, J. Y. Charge Transport in Metal–Oxide Interfaces: Genesis and Detection of Hot Electron Flow and Its Role in Heterogeneous Catalysis. *Catal. Letters* **2015**, *145* (1), 299–308. https://doi.org/10.1007/s10562-014-1418-y.

(49) Niu, H.; Zheng, Y.; Wang, S.; Zhao, L.; Yang, S.; Cai, Y. Continuous Generation of Hydroxyl Radicals for Highly Efficient Elimination of Chlorophenols and Phenols Catalyzed by Heterogeneous Fenton-like Catalysts Yolk/Shell Pd@Fe_3O_4@metal Organic Frameworks. *J. Hazard. Mater.* **2018**, *346*, 174–183. https://doi.org/10.1016/j.jhazmat.2017.12.027.

(50) Lu, J.; Zhang, H.; Li, S.; Guo, S.; Shen, L.; Zhou, T.; Zhong, H.; Wu, L.; Meng, Q.; Zhang, Y. Oxygen-Vacancy-Enhanced Peroxidase-like Activity of Reduced Co_3O_4 Nanocomposites for the Colorimetric Detection of H_2O_2 and Glucose. *Inorg. Chem.* **2020**, *59* (5), 3152–3159. https://doi.org/10.1021/acs.inorgchem.9b03512.

(51) Ma, M.; Xie, J.; Zhang, Y.; Chen, Z.; Gu, N. Fe3O4@Pt Nanoparticles with Enhanced Peroxidase-like Catalytic Activity. *Mater. Lett.* **2013**, *105*, 36–39. https://doi.org/10.1016/j.matlet.2013.04.020.

(52) Nanda, S.; Nanda, K. K. Identifying the Accuracy of Various Approaches for Determining the Fraction of Surface Atoms in a Nanoparticle to Deepen Students' Understanding of Size-Dependent Properties. *J. Chem. Educ.* **2021**, *98* (6), 1982–1987. https://doi.org/10.1021/acs.jchemed.0c01247.

(53) Jia, H.; Du, A.; Zhang, H.; Yang, J.; Jiang, R.; Wang, J.; Zhang, C. Y. Site-Selective Growth of Crystalline Ceria with Oxygen Vacancies on Gold Nanocrystals for Near-Infrared Nitrogen Photofixation. *J. Am. Chem. Soc.* **2019**, *141* (13), 5083–5086. https://doi.org/10.1021/jacs.8b13062.

(54) Naveen Prasad, S.; Weerathunge, P.; Karim, M. N.; Anderson, S.; Hashmi, S.; Mariathomas, P. D.; Bansal, V.; Ramanathan, R. Non-Invasive Detection of Glucose in Human Urine Using a Color-Generating Copper NanoZyme. *Anal. Bioanal. Chem.* **2021**, *413* (5), 1279–1291. https://doi.org/10.1007/s00216-020-03090-w.

(55) Arakha, M.; Pal, S.; Samantarrai, D.; Panigrahi, T. K.; Mallick, B. C.; Pramanik, K.; Mallick, B.; Jha, S. Antimicrobial Activity of Iron Oxide Nanoparticle upon Modulation of Nanoparticle-Bacteria Interface. *Sci. Rep.* **2015**, *5*, 14813. https://doi.org/10.1038/srep14813.

(56) Kim, M. S.; Kweon, S. H.; Cho, S.; An, S. S. A.; Kim, M. Il; Doh, J.; Lee, J. Pt-Decorated Magnetic Nanozymes for Facile and Sensitive Point-of-Care Bioassay. *ACS Appl. Mater. Interfaces* **2017**, *9* (40), 35133–35140. https://doi.org/10.1021/acsami.7b12326.

(57) Bhagat, S.; Srikanth Vallabani, N. V.; Shutthanandan, V.; Bowden, M.; Karakoti, A. S.; Singh, S. Gold Core/Ceria Shell-Based Redox Active Nanozyme Mimicking the Biological Multienzyme Complex Phenomenon. *J. Colloid Interface Sci.* **2018**, *513*, 831–842. https://doi.org/10.1016/j.jcis.2017.11.064.

(58) Liu, H.; Ding, Y.; Yang, B.; Liu, Z.; Liu, Q.; Zhang, X. Colorimetric and Ultrasensitive Detection of H_2O_2 Based on Au/Co_3O_4-CeO_x Nanocomposites with Enhanced Peroxidase-like Performance. *Sensors Actuators, B Chem.* **2018**, *271*, 336–345. https://doi.org/10.1016/j.snb.2018.05.108.

(59) Zandieh, M.; Liu, J. Nanozyme Catalytic Turnover and Self-Limited Reactions. *ACS Nano* **2021**, *15* (10), 15645–15655. https://doi.org/10.1021/acsnano.1c07520.

(60) Gao, L.; Zhuang, J.; Nie, L.; Zhang, J.; Zhang, Y.; Gu, N.; Wang, T.; Feng, J.; Yang, D.; Perrett, S.; Yan, X. Intrinsic Peroxidase-like Activity of Ferromagnetic Nanoparticles. *Nat.*

Nanotechnol. **2007**, *2* (9), 577–583. https://doi.org/10.1038/nnano.2007.260.

SYNOPSIS

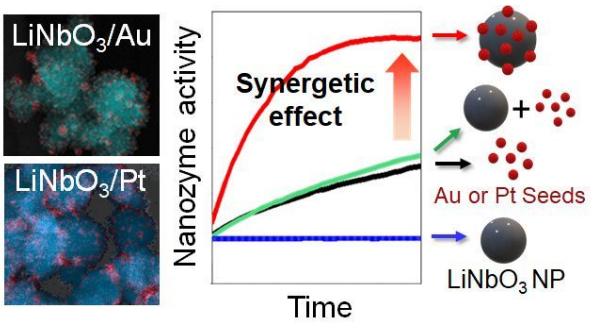

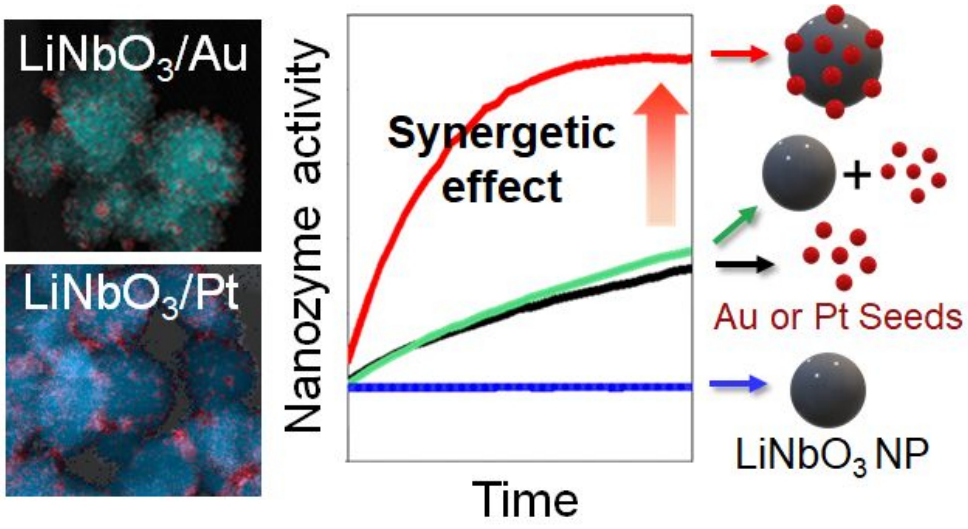

227x125mm (72 x 72 DPI)